

# Sharp enhancement of spin fluctuations by nematic order in iron pnictides

Qiang Zhang,<sup>1,2</sup> Rafael M. Fernandes,<sup>3</sup> Jagat Lamsal,<sup>1,2</sup> Jiaqiang Yan,<sup>4</sup> Songxue Chi,<sup>4</sup> Gregory S. Tucker,<sup>1,2</sup> Daniel K. Pratt,<sup>5</sup> Jeffrey W. Lynn,<sup>5</sup> R. W. McCallum,<sup>1,6</sup> Paul C. Canfield,<sup>1,2</sup> Thomas A. Lograsso,<sup>1,6</sup> Alan I. Goldman,<sup>1,2</sup> David Vaknin,<sup>1,2</sup> and Robert J. McQueeney<sup>1,2,4,\*</sup>

<sup>1</sup>Ames Laboratory, Ames, IA, 50011, USA

<sup>2</sup>Department of Physics and Astronomy, Iowa State University, Ames, IA, 50011, USA

<sup>3</sup>School of Physics and Astronomy, University of Minnesota, Minneapolis, MN 55455, USA

<sup>4</sup>Oak Ridge National Laboratory, Oak Ridge, Tennessee 37831, USA

<sup>5</sup>NIST Center for Neutron Research, National Institute of Standards and Technology, Gaithersburg, Maryland 20899-6102, USA

<sup>6</sup>Department of Materials Sciences and Engineering, Iowa State University, Ames, Iowa 50011, USA

(Dated: December 7, 2024)

Inelastic neutron scattering was employed to investigate the impact of electronic nematic order on the magnetic spectra of LaFeAsO and Ba(Fe<sub>0.953</sub>Co<sub>0.047</sub>)<sub>2</sub>As<sub>2</sub>. These materials are ideal to study the paramagnetic-nematic state, since the nematic order, signaled by the tetragonal-to-orthorhombic transition at  $T_S$ , sets in well above the stripe antiferromagnetic ordering at  $T_N$ . We find that the temperature-dependent dynamic susceptibility displays an anomaly at  $T_S$  followed by a sharp enhancement in the spin-spin correlation length, revealing a strong feedback effect of nematic order on the low-energy magnetic spectrum. Our findings can be consistently described by a model that attributes the structural/nematic transition to magnetic fluctuations, and unveils the key role played by nematic order in promoting the long-range stripe antiferromagnetic order in iron pnictides.

One of the most interesting features of the “122” (e.g. BaFe<sub>2</sub>As<sub>2</sub>) and “1111” (e.g. LaFeAsO) families of iron-based superconductors is the intimate coupling between superconductivity (SC), stripe antiferromagnetic order (AFM), and the tetragonal-to-orthorhombic structural transition [1–5]. For example, in both families, chemical substitutions on the transition metal site, such as Co and Ni, suppress the AFM ordering and the structural transition and, over a limited range of doping, promote SC [4]. For underdoped BaFe<sub>2</sub>As<sub>2</sub>, evidence of a direct competition between AFM and SC has been presented [6–10] in addition to a suppression of the orthorhombic distortion below the superconducting transition temperature  $T_C$  [11, 12]. Despite this competition between SC and long-range magnetic/orthorhombic order, SC generally arises when large AFM/structural fluctuations are present [13], a feature that attests the intricate relationship between these three intertwined phases [14].

While these previous studies have focused on the impact of SC on the magnetic and orthorhombic phases, the interplay between these two ordered states has been a topic of intense debate [15]. For the parent compounds of the “122” family, the magnetic transition temperature ( $T_N$ ) practically coincides with the structural distortion at  $T_S$  [16–18], whereas in the Co-underdoped BaFe<sub>2</sub>As<sub>2</sub> and in the parent compounds of the “1111” family, such as LaFeAsO, the orthorhombic distortion occurs well above  $T_N$  [19, 20]. The structural transition has been proposed to be driven by electronic correlations [21] – associated with either spin [7, 22–24, 26] or charge/orbital degrees of freedom [27–30] – giving rise to the so-called nematic phase in the temperature range between  $T_S$  and  $T_N$ . This electronic nematic phase is characterized not only by a weak in-plane structural anisotropy manifested

by distinct  $a$  and  $b$  lattice constants [11], but also by large in-plane anisotropies in many electronic properties, such as resistivity [21, 31, 32], optical conductivity [33–35], thermopower [36], uniform susceptibility [37, 38], and charge correlations [19, 39, 40]. Previous ARPES [41–44], STM [45, 46], and Raman [47] studies focused on how nematic order affects the normal-state electronic spectrum and, in particular, the charge and orbital degrees of freedom. However, little is known about how nematic order affects the low-energy magnetic fluctuations [48–52], which are particularly important for the formation of the SC state [13].

Here we perform inelastic neutron scattering (INS) experiments to elucidate the evolution of the magnetic spectrum across the nematic transition in single crystals of LaFeAsO and Ba(Fe<sub>0.953</sub>Co<sub>0.047</sub>)<sub>2</sub>As<sub>2</sub>, focusing on the behaviors of the imaginary part of the dynamic magnetic susceptibility  $\chi''(\mathbf{Q}, E)$  and of the spin-spin correlation length  $\xi$  as a function of temperature. These two systems exhibit an orthorhombic distortion whose onset is well separated from the stripe AFM ordering [6, 19, 53, 54], enabling the survival of the nematic phase over a considerable temperature range. Our measurements in twinned samples find clear anomalies in the magnetic spectrum at  $T_S$ . In particular, we find that not only is the overall low-energy magnetic intensity enhanced below  $T_S$ , but also that the spin-spin correlation length undergoes a sharp increase at the nematic transition temperature, in contrast with what one expects from a typical AFM system. This effect reveals a cooperative relationship between nematicity and magnetism, in agreement with theoretical predictions from models that attribute the nematic transition to a spontaneous symmetry breaking driven by magnetic fluctuations [7, 22–24, 26].

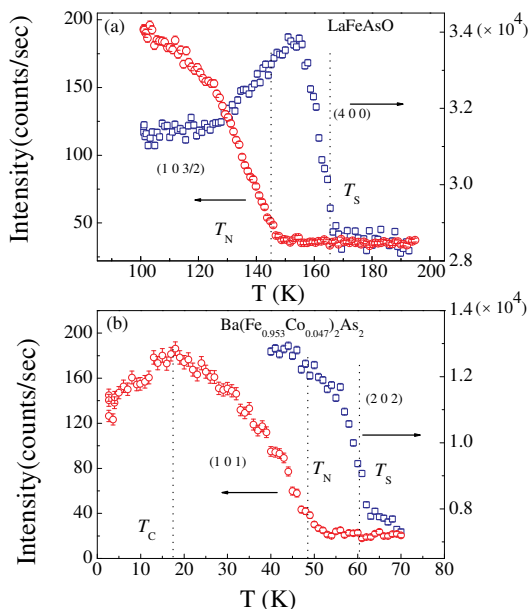


FIG. 1: (color online) (a) Neutron diffraction peak intensities of the  $(1\ 0\ 3/2)$  magnetic reflection and the  $(4\ 0\ 0)/(0\ 4\ 0)$  Bragg reflection as a function of temperature in LaFeAsO. (b) Neutron diffraction peak intensities of the  $(1\ 0\ 1)$  magnetic reflection and the  $(2\ 0\ 2)/(0\ 2\ 2)$  Bragg reflection as a function of temperature in Ba(Fe<sub>0.953</sub>Co<sub>0.047</sub>)<sub>2</sub>As<sub>2</sub>.

The LaFeAsO and Ba(Fe<sub>0.953</sub>Co<sub>0.047</sub>)<sub>2</sub>As<sub>2</sub> crystals were grown using a flux technique as previously described [53, 54]. Dozens of small single-crystals of LaFeAsO with a total mass of approximately 600 mg were co-aligned in the  $(HOL)$  plane within  $\sim 2$  degrees mosaicity. Hereafter, unless otherwise noted with a subscript “T”, we use orthorhombic notation. A large single crystal of Ba(Fe<sub>0.953</sub>Co<sub>0.047</sub>)<sub>2</sub>As<sub>2</sub> with a mass of  $\approx 700$  mg was also aligned in the  $(HOL)$  plane for the investigation. The elastic and inelastic neutron measurements on LaFeAsO and Ba(Fe<sub>0.953</sub>Co<sub>0.047</sub>)<sub>2</sub>As<sub>2</sub> were performed on the HB3 spectrometer (located at the High Flux Isotope Reactor at Oak Ridge National Laboratory) and BT-7 triple-axis neutron spectrometer at the NIST Center for Neutron Research [55], respectively.

In LaFeAsO, neutron diffraction measurements of the  $(1\ 0\ 3/2)$  magnetic Bragg reflection and the  $(4\ 0\ 0)/(0\ 4\ 0)$  nuclear Bragg reflection as a function of temperature show a structural transition at  $T_S=165$  K split from the magnetic transition at  $T_N=145$  K, as illustrated in Fig 1 (a), and consistent with previous reports [19, 53, 56, 57]. The  $(4\ 0\ 0)/(0\ 4\ 0)$  reflection, which develops from the  $(2\ 2\ 0)_T$  tetragonal Bragg reflection, was used to monitor the structural transition indirectly by virtue of secondary extinction changes resulting from the structural transition. Similarly, in Ba(Fe<sub>0.953</sub>Co<sub>0.047</sub>)<sub>2</sub>As<sub>2</sub>, the intensity of the  $(2\ 0\ 2)/(0\ 2\ 2)$  nuclear Bragg reflection indicates that the structural transition occurs at  $T_S = 60$

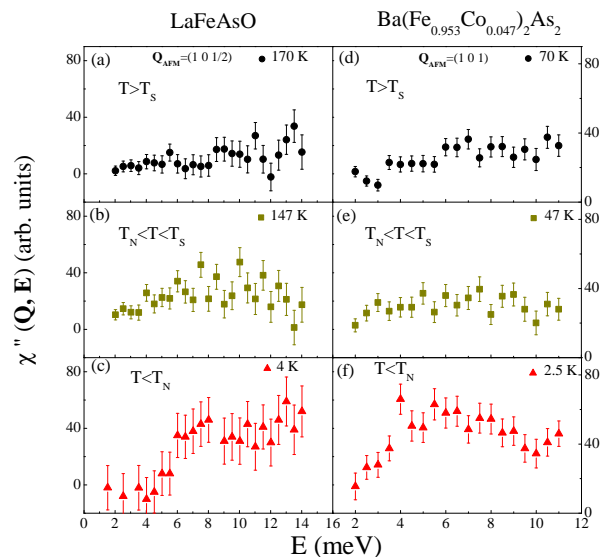


FIG. 2: (color online) Low-energy spin excitation in LaFeAsO at (a) 170 K, (b) 147 K, (c) 4 K and in Ba(Fe<sub>0.953</sub>Co<sub>0.047</sub>)<sub>2</sub>As<sub>2</sub> at (d) 70 K, (e) 47 K, (f) 2.5 K. The results are derived from the difference between a constant-Q energy scan at  $\mathbf{Q}_{\text{AFM}}$  and a background scan at  $\mathbf{Q}'=(0.7\ 0\ 1)$  for Ba(Fe<sub>0.953</sub>Co<sub>0.047</sub>)<sub>2</sub>As<sub>2</sub> and at  $\mathbf{Q}'=(0.83\ 0\ 0.998)$  after the crystal was rotated from nominal  $\mathbf{Q}_{\text{AFM}}$  by  $20^\circ$  for LaFeAsO. The intensities have been normalized to reflect a counting time of approximately five minutes. Error bars where indicated represent one standard deviation.

K, which is split from the magnetic transition at  $T_N = 47$  K according to the  $(1\ 0\ 1)$  magnetic Bragg reflection. The anomalous decrease of the intensity of the  $(1\ 0\ 1)$  magnetic peak below  $T_C \approx 17$  K marks the reduction of the AFM order parameter due to competition with the SC state [6]. The locations of these three transitions in Ba(Fe<sub>0.953</sub>Co<sub>0.047</sub>)<sub>2</sub>As<sub>2</sub> are also consistent with previous reports [39, 54].

To determine the impact of nematic order on the magnetic spectrum, we explore the dependence of the imaginary part of the dynamic susceptibility  $\chi''(\mathbf{Q}, E)$  on the energy  $E$ , the momentum  $\mathbf{Q}$ , and the temperature  $T$ . This quantity is extracted via the relationship:

$$S(\mathbf{Q}, E) \propto f^2(Q)\chi''(\mathbf{Q}, E)(1 - e^{-E/k_B T})^{-1} \quad (1)$$

where  $S(\mathbf{Q}, E)$  is the measured background-subtracted intensity  $I(\mathbf{Q}, E) - B(\mathbf{Q}', E)$ ,  $f(Q)$  is the magnetic form factor of Fe<sup>2+</sup>, and  $k_B$  is the Boltzmann constant. Figure 2 shows  $\chi''(\mathbf{Q}_{\text{AFM}}, E)$  at the magnetic reflection  $\mathbf{Q}_{\text{AFM}}=(1\ 0\ 1/2)$  in LaFeAsO and  $\mathbf{Q}_{\text{AFM}}=(1\ 0\ 1)$  in Ba(Fe<sub>0.953</sub>Co<sub>0.047</sub>)<sub>2</sub>As<sub>2</sub> at several temperatures. Below  $T_N$ , the spectra in LaFeAsO exhibit the onset of an energy gap  $\sim 5$  meV, consistent with previous reports [56]. In Ba(Fe<sub>0.953</sub>Co<sub>0.047</sub>)<sub>2</sub>As<sub>2</sub>, a heavily overdamped energy gap  $\sim 10$  meV [58] is observed. It has been reported [58] that upon the increase of Co substitution in Ba(Fe<sub>1-x</sub>Co<sub>x</sub>)<sub>2</sub>As<sub>2</sub>, the spin gap appears to

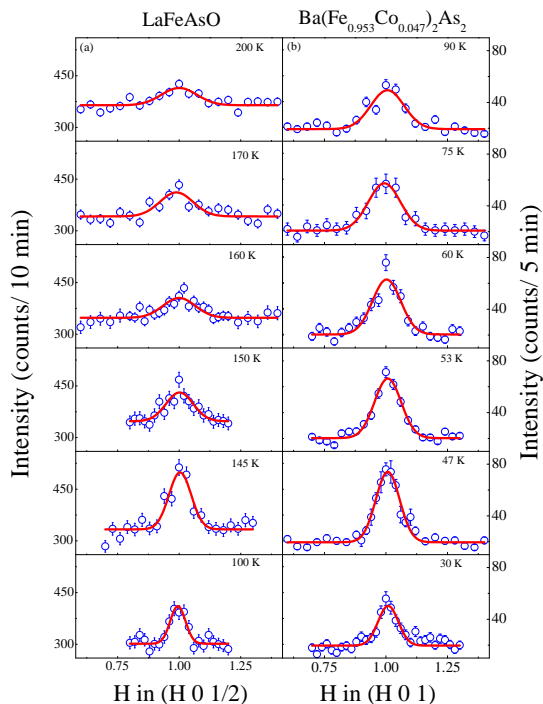


FIG. 3: (Color online) Representative longitudinal  $H$  scans (a) through  $\mathbf{Q}_{\text{AFM}} = (1\ 0\ 1/2)$  at  $E = 5$  meV and various temperatures in LaFeAsO and (b) through  $\mathbf{Q}_{\text{AFM}} = (1\ 0\ 1)$  at  $E = 3$  meV and various temperatures in  $\text{Ba}(\text{Fe}_{0.953}\text{Co}_{0.047})_2\text{As}_2$ . The solid lines are obtained by the best fit to the data to a Gaussian function.

close gradually and is completely absent at  $x=0.055$  due to the crossover from well-defined spin waves to overdamped spin excitations. The spin gaps in both systems vanish above  $T_N$  and the energy-dependent damping also increases above  $T_N$ . These results guide us to measure  $\chi''(\mathbf{Q}, E)$  at a fixed energy transfer of  $E = 5$  meV in LaFeAsO and,  $E = 3$  meV in  $\text{Ba}(\text{Fe}_{0.953}\text{Co}_{0.047})_2\text{As}_2$  to obtain both the spin-spin correlation length and the magnetic intensity as a function of temperature, according to the model for spin fluctuations described in Ref. [58].

Representative longitudinal  $H$  scans through  $\mathbf{Q}_{\text{AFM}} = (1\ 0\ 1/2)$  in LaFeAsO and  $\mathbf{Q}_{\text{AFM}} = (1\ 0\ 1)$  in  $\text{Ba}(\text{Fe}_{0.953}\text{Co}_{0.047})_2\text{As}_2$  at low energy transfers are shown in Fig. 3. The solid lines represent Gaussian fits to the data, as justified in the Supplemental Material. We note that upon decreasing the temperature below  $T_S$ , the lineshape narrows and the peak amplitude increases. The dynamic susceptibility and linewidth (full width at half maximum) versus temperature are shown in Fig. 4. Note that the reasonable mosaicity within  $\sim 2^\circ$  of the coaligned LaFeAsO samples does not appreciably affect the linewidth of longitudinal scans and thus the linewidth reflects the intrinsic behavior of spin-spin correlation length similar to that of  $\text{Ba}(\text{Fe}_{0.953}\text{Co}_{0.047})_2\text{As}_2$ . The dynamic susceptibility shows a discontinuous increase below  $T_S$  (much stronger for LaFeAsO) and exhibits a maxi-

mum at the AFM ordering temperature  $T_N$ , followed by a gradual decrease below  $T_N$  due to the opening of the spin gap. As shown in Fig. 4 (b) and (d), the linewidth decreases as  $T$  approaches  $T_N$ , which is expected for a classic second-order AFM phase transition. The striking result of this study is the observation of a sharp decrease in the linewidth below  $T_S$  in both LaFeAsO and  $\text{Ba}(\text{Fe}_{0.953}\text{Co}_{0.047})_2\text{As}_2$  systems, which signifies a strong effect of nematic order on the approach to AFM order.

Above the magnetic transition temperature  $T_N$ , the linewidth of the constant-energy  $Q$  scans is proportional to the inverse magnetic correlation length  $\xi^{-1}$  associated with the paramagnetic fluctuations [58, 59] (also see the Supplemental Material). Therefore, the onset of long-range nematic order promotes a strong increase of this correlation length, enhancing the tendency of the system towards long-range magnetic order. Such a cooperative interplay between nematicity and magnetism can be understood qualitatively within models that attribute the tetragonal symmetry-breaking to magnetic fluctuations emerging from either localized [22, 23] or itinerant spins [7]. To illustrate the corresponding microscopic mechanism, we show schematically in Fig. 5(a) the evolution of the magnetic fluctuations across  $T_S$  and  $T_N$  both in real space (upper panels) and in spin space (lower panels). The crucial point behind this mechanism is that the iron pnictides display two degenerate stripe AFM ground states, with ordering vectors  $\mathbf{Q}_1 = (1\ 0\ L)$  and  $\mathbf{Q}_2 = (0\ 1\ L)$ . Thus, the magnetic ground state can be described in terms of two interpenetrating square sublattices – associated with the two distinct Fe atoms in the unit cell – that tend to order magnetically in Néel-like configurations (blue and red dashed lines in Fig. 5(a)).

Above  $T_S$ , where there is no long-range magnetic order, these two sublattices are essentially independent (as shown in the upper left panel of Fig. 5(a)), and their fluctuations are uncoupled (as shown in the lower left panel). As a result, the system has multiple possible ground states, a feature commonly seen in frustrated spin systems with low magnetic transition temperatures. However, below  $T_S$  but above  $T_N$ , nematic order emerges as a coupling between the two sublattices (upper middle panel in Fig. 5(a)), enforcing the two corresponding Néel order parameters to fluctuate coherently either antiparallel (as shown in the lower middle panel) or parallel to each other. There is still no long-range magnetic order, since the spins can point at any direction in spin space. However, the tetragonal symmetry of the system is broken, since nearest-neighbor spins are locked in a ferromagnetic-like or an antiferromagnetic-like configuration. Furthermore, by breaking the tetragonal symmetry, nematic order reduces the number of possible magnetic ground states to only one – either the  $\mathbf{Q}_1 = (1\ 0\ L)$  stripe if the  $a$  direction is selected along the  $x$  axis, or the  $\mathbf{Q}_2 = (0\ 1\ L)$  stripe if the  $a$  direction is selected along the  $y$  direction. Thus, the frustration present at higher

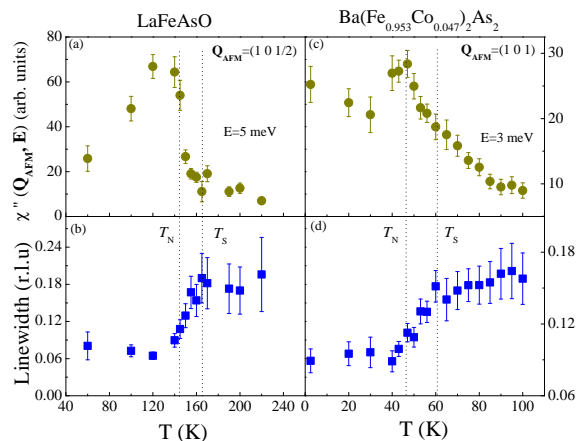


FIG. 4: (color online) Temperature dependence of (a) dynamic susceptibility  $\chi''(\mathbf{Q}, E = 5 \text{ meV})$  and (b) the Gaussian linewidth, obtained by fitting the longitudinal H scans through  $\mathbf{Q}_{\text{AFM}} = (1 \ 0 \ 1/2)$  at  $E = 5 \text{ meV}$  in LaFeAsO. Temperature dependence of (c) the dynamic susceptibility  $\chi''(\mathbf{Q}, E = 3 \text{ meV})$  and (d) the Gaussian linewidth, obtained by fitting the longitudinal H scans through  $\mathbf{Q}_{\text{AFM}} = (1 \ 0 \ 1)$  at  $E = 3 \text{ meV}$  in  $\text{Ba}(\text{Fe}_{0.953}\text{Co}_{0.047})_2\text{As}_2$ . The vertical dashed lines mark the locations of the structural transition  $T_S$  and the AFM magnetic transition  $T_N$ .

temperatures is lifted by nematic order, resulting in an enhancement of the spin-spin correlation length  $\xi$ , and therefore of  $T_N$ , which sets in when  $\xi$  diverges (right panels). Note that this phenomenon can be observed even in twinned samples as the ones studied here, since magnetic fluctuations are enhanced regardless of the type of nematic domain selected.

To go beyond this qualitative analysis, we calculate  $\xi$  using a low-energy action for the magnetic degrees of freedom that accounts for the existence of two symmetry-related magnetic instabilities which give rise to a preemptive nematic phase at  $T_S > T_N$  (see Ref. [7] for a microscopic derivation from an itinerant 3-band model). The equations for  $\xi$  and the parameters used here are presented in the Supplemental Material. To take into account the resolution limitations in the linewidth  $W$  imposed by the instrument and by the fact that the measurements are performed at non-zero energy, we shift  $\xi^{-1}$  by a temperature-independent term  $\delta_{\text{res}} > 0$ ,  $W \propto \xi^{-1} + \delta_{\text{res}}$ . The results are shown in Fig. 5(b). Because our model is based on an expansion near  $T_N$ , it systematically underestimates the correlation length at higher temperatures. Yet, it captures the main qualitative feature observed experimentally, namely, the sharp enhancement of  $\xi$  below  $T_S$  due to the onset of long-range nematic order. This is shown explicitly in Fig. 5b by comparing the hypothetical behavior of  $\xi$  in the absence of nematic order (dashed lines) with the behavior in the presence of nematicity (solid lines). We emphasize that this theoretical calculation is intended to highlight the

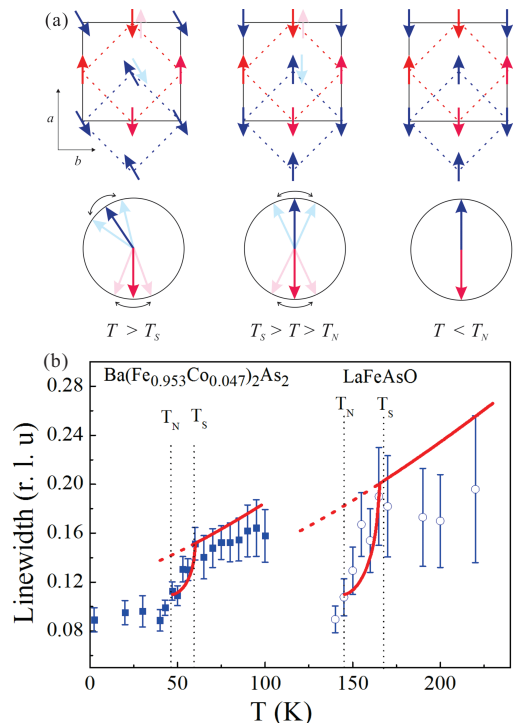


FIG. 5: (color online) (a) Evolution of the magnetic fluctuations of the iron pnictides in real space (upper panels) and spin space (lower panels). The two Néel sublattices corresponding to the two different Fe atoms of the unit cell (dashed lines) are shown in red and blue. Above  $T_N$ , spins in each sublattice fluctuate around a Néel configuration. These fluctuations are uncoupled above  $T_S$ , but below  $T_S$ , the two fluctuating Néel sublattices are coupled either parallel or anti-parallel to each other. The double arrows in the upper panels represent fluctuating spins, as explicitly shown in the lower panels. Below  $T_N$ , spins point to a fixed direction in spin space. (b) Temperature dependence of the theoretical linewidth  $W$  (red lines) compared to the experimental linewidth (blue dots). The dashed lines mark the locations of  $T_S$  and  $T_N$  in LaFeAsO and  $\text{Ba}(\text{Fe}_{0.953}\text{Co}_{0.047})_2\text{As}_2$ .

strong feedback effect of nematic order on the magnetic fluctuations, and not to capture the full quantitative dependence of  $\xi$  on temperature, which will be affected by other features such as domains, mosaicity, etc.

In summary, we have reported unambiguous evidence for the feedback effect of nematic order on the magnetic spectrum in both “1111” and underdoped “122” families of the iron pnictides with  $T_S > T_N$ , manifested by the sharp enhancement of the spin-spin correlation length below  $T_S$ , revealing a key impact of this elusive electronic order on the normal-state properties of the iron arsenides. Since magnetic fluctuations are believed to be important for the formation of the SC state [13], and our results provide evidence that nematic order enhances them, this suggests that nematicity may be more than another competing order, as previously reported [11, 12], and may even help enhancing  $T_C$  in some circumstances [60, 61].

*Acknowledgements.* Research at Ames Laboratory is supported by the US Department of Energy, Office of Basic Energy Sciences, Division of Materials Sciences and Engineering under Contract No. DE-AC02-07CH11358. R.M.F. is supported by the Department of Energy under Award Number DE-SC0012336. Use of the high flux isotope reactor at the Oak Ridge National Laboratory, was supported by the US Department of Energy, Office of Basic Energy Sciences, Scientific User Facilities Division. The NIST Center for Neutron Research is supported by the US Department of Commerce. We acknowledge Dan Parshall for his technical assistance in measuring  $\text{Ba}(\text{Fe}_{0.953}\text{Co}_{0.047})_2\text{As}_2$  at BT-7 triple-axis neutron spectrometer at the NIST center for Neutron Research.

---

\* Electronic address: mcqueeneyrj@ornl.gov

- [1] K. Ishida, Y. Nakai and H. Hosono, *J. Phys. Soc. Japan* **78**, 062001 (2009).
- [2] D. C. Johnston, *Adv. Phys.* **59**, 803 (2010)
- [3] J. Paglione and R. L. Greene, *Nature Phys.* **6**, 645 (2010)
- [4] P. C. Canfield and S. L. Bud'ko, *Annu. Rev. Cond. Mat. Phys.* **1**, 27 (2010)
- [5] H. H. Wen and S. Li, *Annu. Rev. Cond. Mat. Phys.* **2**, 121 (2011).
- [6] D. K. Pratt, W. Tian, A. Kreyssig, J. L. Zarestky, S. Nandi, N. Ni, S. L. Bud'ko, P. C. Canfield, A. I. Goldman, and R. J. McQueeney, *Phys. Rev. Lett.* **103**, 087001 (2009).
- [7] A. D. Christianson, M. D. Lumsden, S. E. Nagler, G. J. MacDougall, M. A. McGuire, A. S. Sefat, R. Jin, B. C. Sales, and D. Mandrus, *Phys. Rev. Lett.* **103**, 087002 (2009).
- [8] R. M. Fernandes *et al.*, *Phys. Rev. B* **81**, 140501(R) (2010).
- [9] S. Avci, O. Chmaissem, E. A. Goremychkin, S. Rosenkranz, J.-P. Castellan, D. Y. Chung, I. S. Todorov, J. A. Schlueter, H. Claus, M. G. Kanatzidis, A. Daoud-Aladine, D. Khalyavin, and R. Osborn, *Phys. Rev. B* **83**, 172503 (2011).
- [10] Huiqian Luo, Rui Zhang, Mark Laver, Zahra Yamani, Meng Wang, Xingye Lu, Miaoyin Wang, Yanchao Chen, Shiliang Li, Sung Chang, Jeffrey W. Lynn, and Pengcheng Dai, *Phys. Rev. Lett.* **108**, 247002 (2012).
- [11] S. Nandi *et al.*, *Phys. Rev. Lett.* **104**, 057006 (2010).
- [12] A. E. Böhrer, P. Burger, F. Hardy, T. Wolf, P. Schweiss, R. Fromknecht, H. v. Löhneysen, C. Meingast, H. K. Mak, R. Lortz, S. Kasahara, T. Terashima, T. Shibauchi, and Y. Matsuda, *Phys. Rev. B* **86**, 094521 (2012).
- [13] P. J. Hirschfeld, M. M. Korshunov, and I. I. Mazin, *Rep. Prog. Phys.* **74**, 124508 (2011); A. V. Chubukov, *Annu. Rev. Cond. Mat. Phys.* **3**, 57 (2012).
- [14] E. Fradkin, S. A. Kivelson, and J. M. Tranquada, arXiv:1407.4480 (2014).
- [15] R. M. Fernandes, A. V. Chubukov, and J. Schmalian, *Nature Phys.* **10**, 97 (2014).
- [16] H.-F. Li, *et al.*, *Phys. Rev. B* **80**, 054407 (2009).
- [17] M. G. Kim, *et al.*, *Phys. Rev. B* **83**, 134522 (2011).
- [18] C. R. Rotundu and R. J. Birgeneau, *Phys. Rev. B* **84**, 092501 (2011).
- [19] H.-F. Li, *et al.*, *Phys. Rev. B* **82**, 064409 (2010).
- [20] Q. Zhang, *et al.*, *Phys. Rev. B* **88**, 174517 (2013).
- [21] J.-H. Chu, H.-H. Kuo, J. G. Analytis, and I. R. Fisher, *Science* **337**, 710 (2012).
- [22] C. Fang, H. Yao, W.-F. Tsai, J. Hu, and S. A. Kivelson, *Phys. Rev. B* **77**, 224509 (2008).
- [23] C. Xu, M. Muller, and S. Sachdev, *Phys. Rev. B* **78**, 020501 (2008).
- [24] R. M. Fernandes, *et al.*, *Phys. Rev. Lett.* **105**, 157003 (2010).
- [25] R. M. Fernandes, A. V. Chubukov, J. Knolle, I. Eremin, and J. Schmalian, *Phys. Rev. B* **85**, 024534 (2011).
- [26] S. Liang, A. Moreo, and E. Dagotto, *Phys. Rev. Lett.* **111**, 047004 (2013).
- [27] C. C. Lee, W. G. Yin, and W. Ku, *Phys. Rev. Lett.* **103**, 267001 (2009).
- [28] C.-C. Chen, J. Maciejko, A. P. Sorini, B. Moritz, R. R. P. Singh, and T. P. Devereaux, *Phys. Rev. B* **82**, 100504 (2010).
- [29] W.-C. Lee and P. W. Phillips, *Phys. Rev. B* **86**, 245113 (2012).
- [30] S. Onari H. and Kontani, *Phys. Rev. Lett.* **109**, 137001 (2012).
- [31] J.-H. Chu, *et al.*, *Science* **329**, 824 (2010).
- [32] M. A. Tanatar *et al.*, *Phys. Rev. B* **81**, 184508 (2010).
- [33] A. Dusza *et al.*, *Europhys. Lett.* **93**, 37002 (2011).
- [34] M. Nakajima *et al.*, *Proc. Natl. Acad. Sci. U.S.A.* **108**, 12238-12242 (2011).
- [35] A. Patz, *et al.*, *Nature Comm.* **5**, 3229 (2014).
- [36] S. Jiang *et al.*, *Phys. Rev. Lett.* **110**, 067001 (2013).
- [37] S. Kasahara, *et al.*, *Nature* **486**, 382 (2012).
- [38] Xiaofeng Xu *et al.*, *Phys. Rev. B* **89**, 104517 (2014).
- [39] Q. Zhang, *et al.*, *Phys. Rev. B* **87**, 094510 (2013).
- [40] Y. K. Kim *et al.*, *Phys. Rev. Lett.* **111**, 217001 (2013).
- [41] M. Yi, *et al.*, *Proc. Nat. Acad. Sci.* **108**, 6878 (2011).
- [42] Y. Zhang *et al.*, *Phys. Rev. B* **85**, 085121 (2012).
- [43] M Yi *et al.*, *New J. Phys.* **14**, 073019 (2012).
- [44] T. Shimojima *et al.*, *Phys. Rev. B* **89**, 045101 (2014).
- [45] T.-M. Chuang *et al.*, *Science* **327**, 181-184 (2010).
- [46] E. P. Rosenthal *et al.*, *Nature Phys.* **10**, 225 (2014).
- [47] Y. Gallais *et al.*, *Phys. Rev. Lett.* **111**, 267001 (2013).
- [48] L. Ma *et al.*, *Phys. Rev. B* **83**, 132501 (2011).
- [49] M. Fu *et al.*, *Phys. Rev. Lett.* **109**, 247001 (2012).
- [50] Y. Song *et al.*, *Phys. Rev. B* **88**, 134512 (2013).
- [51] H. Luo *et al.*, *Phys. Rev. Lett.* **111**, 107006 (2013).
- [52] X. Lu *et al.*, *Science* **345**, 657 (2014).
- [53] J.-Q. Yan, *et al.*, *Appl. Phys. Lett.*, **95**, 222504 (2009).
- [54] N. Ni, M. E. Tillman, J.-Q. Yan, A. Kracher, S. T. Hannahs, S. L. Bud'ko, and P. C. Canfield, *Phys. Rev. B* **78**, 214515 (2008).
- [55] J. W. Lynn, *et al.*, *Journal of Research of NIST*, **117**, 61-79 (2012).
- [56] M. Ramazanoglu, *et al.*, *Phys. Rev. B* **87**, 140509 (2013).
- [57] C. A. McElroy, *et al.*, *Phys. Rev. B* **88**, 134513 (2013).
- [58] G. S. Tucker, *et al.*, *Phys. Rev. B* **89**, 180503(R) (2014).
- [59] M. Kofu, *et al.*, *Phys. Rev. Lett.* **102**, 047001. (2009); M. Steiner, *et al.*, *J. Phys. C: Solid State Phys.*, **8**, 165. (1975)
- [60] R. M. Fernandes and A. J. Millis, *Phys. Rev. Lett.* **111**, 127001 (2013).
- [61] F. Yang, F. Wang, and D.-H. Lee, *Phys. Rev. B* **88**, 100504 (2013).

Supplementary material for: “Sharp enhancement of spin fluctuations by nematic order in iron pnictides”

### I. LINEWIDTH FITS

In this Supplemental section, we provide more details on the justification of the Gaussian fit performed to the constant-energy longitudinal scans presented in Fig. 3 of the article. In the main text, we identified the Gaussian linewidth with the inverse magnetic correlation length. This is justified because the energy probed is much smaller than the damping of the magnetic excitations present in the paramagnetic state.

To make this point clearer, we use the microscopically-derived diffusive model discussed in Refs. [1–4] that captures the low-energy magnetic excitations near the magnetic ordering vector  $\mathbf{Q}$ . Within this model, the in-plane dynamic magnetic susceptibility is given by (in tetragonal notation):

$$\chi(\mathbf{q} + \mathbf{Q}_{\text{AFM}}, E) = \frac{\chi_0}{a^2 (\xi^{-2} + q_x^2 + q_y^2 + \eta q_x q_y) - iE\gamma} \quad (2)$$

where  $\chi_0^{-1}$  is an overall magnetic energy scale,  $\xi$  is the magnetic correlation length,  $E$  is the energy,  $\mathbf{q}$  is the reduced momentum,  $a$  is the lattice constant,  $\eta$  is the in-plane anisotropy parameter, and  $\gamma$  is the Landau damping. This expression is derived from an effective three-band model and ultimately relies on the fact that the paramagnetic excitations can decay into particle-hole excitations, giving rise to Landau damping. The comparison with the spin-spin correlation function  $S(\mathbf{Q}, E)$ , extracted in the inelastic neutron scattering (INS) experiments, is achieved via the fluctuation-dissipation theorem:

$$S(\mathbf{Q}, E) \propto \left(1 - e^{-E/k_B T}\right)^{-1} \text{Im}[\chi(\mathbf{Q}, E)] \quad (3)$$

Previously, Eq.(2) has been successfully employed to fit the experimental INS data in the paramagnetic state across the entire phase diagram of the  $\text{Ba}(\text{Fe}_{1-x}\text{Co}_x)_2\text{As}_2$  compounds [2–4]. In particular, the only temperature-dependent parameter is the correlation length  $\xi$ , while  $\eta$  and  $\gamma$  depend only on the Co concentration  $x$ .

To check whether the effective Gaussian model used to fit the data of the  $x = 0.047$  sample (taken at  $E = 3$  meV and shown in the right column of Fig. 3 of the main text) is consistent with the microscopically-derived diffusive model, we use the temperature-independent parameters reported in Ref. [3] for  $x = 0.047$ ,  $\eta = 1.14$  and

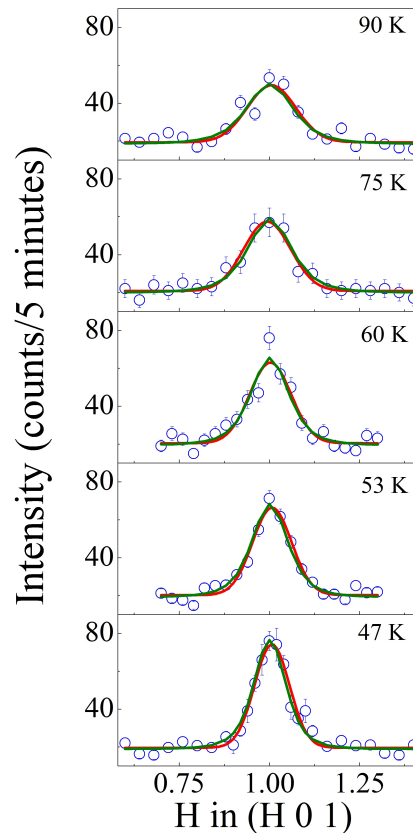


FIG. 6: (color online) Comparison of two types of fits using a Gaussian function (red solid line) and the diffusive model of Eq. (2) (olive solid line) to the experimental data (open circles) in  $\text{Ba}(\text{Fe}_{0.953}\text{Co}_{0.047})_2\text{As}_2$ .

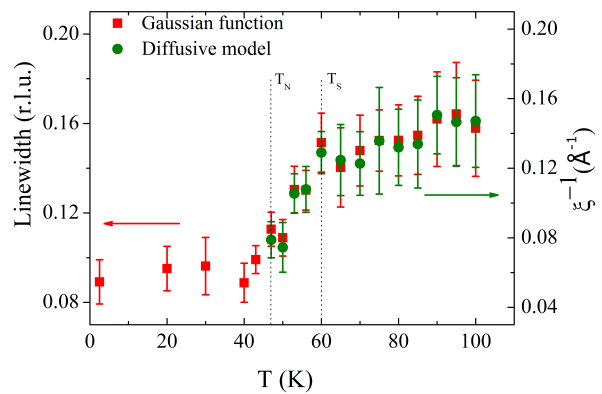


FIG. 7: (color online) Comparison of the temperature dependence of the inverse spin-spin correlation length  $\xi^{-1}$  derived from the diffusive model of Eq. (2) (olive circles) and the linewidth obtained from the Gaussian function fits (red squares) in  $\text{Ba}(\text{Fe}_{0.953}\text{Co}_{0.047})_2\text{As}_2$ . The vertical dashed lines mark the positions of  $T_S$  and  $T_N$ .

$\gamma^{-1} = 75$  meV, and extract the temperature dependence of the magnetic correlation length  $\xi$  by fitting the experimental INS intensity corrected for the Bose thermal population factor and the  $\text{Fe}^{2+}$  single-ion magnetic form factor to Eq. (2) after convolution with the Popovici approximation to the instrumental resolution using the RESLIB program [5]. The fits for several temperatures are shown in Fig. 6, and the temperature dependence of the inverse spin-spin correlation length is shown in Fig. 7. Comparison with the fits to the effective Gaussian model are also presented in both figures, revealing that indeed the Gaussian linewidth correctly captures the temperature dependence of the inverse correlation length and, in particular, its sharp suppression below  $T_S$ . Note that because this model is appropriate only for the paramagnetic phase, the fittings were only performed above  $T_N$ .

The reason behind this agreement between the two models can be understood directly from Eqs. (2) and (3). In particular, since  $E\gamma \approx 0.04 \ll 1$ , the behavior of  $\text{Im}[\chi(\mathbf{q}, E)]$  is dominated by the static part, which, due to the convolution with the experimental resolution, is well captured by an effective Gaussian curve. For LaFeAsO, a systematic fitting of the INS data in the paramagnetic state to the diffusive model Eq. (2) is not available. Nevertheless, because the damping factors in the magnetically ordered states of both LaFeAsO and  $\text{Ba}(\text{Fe}_{0.953}\text{Co}_{0.047})_2\text{As}_2$  have similar magnitudes [6], it is not unreasonable to expect the same to be true in the paramagnetic state. In this case,  $E\gamma \ll 1$  would also be true in LaFeAsO, justifying the use of an effective Gaussian curve to fit the constant-energy longitudinal scans.

## II. THEORETICAL MODEL

The theoretical model presented in the main text for the temperature dependence of the correlation length  $\xi$  was derived previously in Ref. [7]. The key ingredient of this model is the existence of two magnetic instabilities at the ordering vectors  $\mathbf{Q}_1 = (\pi, 0)$  and  $\mathbf{Q}_2 = (0, \pi)$  (in units of the square Fe lattice parameter). The two corresponding order parameters are denoted by  $\mathbf{M}_1$  and  $\mathbf{M}_2$ , and the magnetic action is given by:

$$S[\mathbf{M}_i] = \int_q \chi_q^{-1} (M_1^2 + M_2^2) + \frac{u}{2} \int_x (M_1^2 + M_2^2)^2 - \frac{g}{2} \int_x (M_1^2 - M_2^2)^2 \quad (4)$$

where  $\int_q = T \sum_{\omega_n} \int \frac{d^d q}{(2\pi)^d}$  and  $\int_x = \int_0^\beta d\tau \int d^d x$ . Here  $u > g > 0$  are phenomenological parameters that can in principle be derived from a microscopic 3-band model [7], and  $\chi_q^{-1} = r_0 + q^2$  for a classical phase transition, with  $r_0$  a temperature-dependent tuning parameter. Within this model, the nematic order parameter, given by  $\varphi =$

$g \langle M_1^2 - M_2^2 \rangle$ , can condense at a temperature above the magnetic transition temperature, breaking the tetragonal symmetry of the system, since  $\mathbf{M}_1$  and  $\mathbf{M}_2$  are related by a  $90^\circ$  rotation. Thus, from this action, one can derive the behavior of the magnetic correlation length  $\xi$  across the nematic phase transition. In the large- $N$  approach, where Gaussian magnetic fluctuations are included self-consistently, one obtains two coupled non-linear equations for the parameters  $r$  and  $\varphi$ :

$$r = \bar{r}_0 - \frac{\bar{u}}{4} \left[ (r + \varphi)^{\frac{d-2}{2}} + (r - \varphi)^{\frac{d-2}{2}} \right] \\ \varphi = \frac{\bar{g}}{4} \left[ (r + \varphi)^{\frac{d-2}{2}} - (r - \varphi)^{\frac{d-2}{2}} \right] \quad (5)$$

where  $d$  is the dimensionality and  $\bar{u}$ ,  $\bar{g}$ ,  $\bar{r}_0$  are the corresponding renormalized parameters of the original action. The magnetic correlation length can be obtained via  $\xi^{-2} \propto r - \varphi$ . It is clear, in this regard, the origin of the kink observed in  $\xi$ : it arises because, above  $T_S$ ,  $\varphi = 0$ , whereas below  $T_S$ ,  $\varphi \neq 0$ . In particular, introducing the auxiliary variable  $z = \varphi/r$ , the magnetic correlation length is given by:

$$\xi^{-1} = A \sqrt{\left[ \frac{(1+z)^{\frac{d-2}{2}} - (1-z)^{\frac{d-2}{2}}}{z} \right]^{\frac{2}{4-d}} (1-z)} \quad (6)$$

where  $A$  is a positive constant and  $z$  is determined implicitly as function of  $\bar{r}_0 \rightarrow \bar{r}_0 / \left(\frac{g}{4}\right)^{\frac{2}{4-d}}$  according to:

$$\bar{r}_0 = \left[ \frac{(1+z)^{\frac{d-2}{2}} - (1-z)^{\frac{d-2}{2}}}{z} \right]^{\frac{d-2}{4-d}} \times \left[ (1+z)^{\frac{d-2}{2}} \left( \alpha + \frac{1}{z} \right) + (1-z)^{\frac{d-2}{2}} \left( \alpha - \frac{1}{z} \right) \right] \quad (7)$$

where  $\alpha \equiv u/g$ . As shown explicitly in Ref. [7], to mimic the interlayer coupling in the iron pnictides, one can consider an intermediate dimensionality  $2 < d < 3$ . The theoretical results presented in Fig. 5 of the main text were obtained by solving Eqs. (6) and (7) for  $d = 2.6$  and the following set of parameters: for LaFeAsO, we used  $\alpha = 17$ ,  $\bar{r}_0 = 0.18 (T - 9.3)$ , and  $A = 0.13$ ; for  $\text{Ba}(\text{Fe}_{0.953}\text{Co}_{0.047})_2\text{As}_2$  we used  $\alpha = 30$ ,  $\bar{r}_0 = 0.54 (T + 30.9)$ , and  $A = 0.06$ .

As explained in the main text and in the previous section of the Supplemental Material, the linewidth  $W$  measured experimentally is limited by both the instrument resolution and by the fact that the measurements were performed at non-zero energies  $E > 0$ . For instance, from Eq. (2) we note that even when  $\xi \rightarrow \infty$ , the spin-spin correlation function acquires effectively a finite linewidth, according to:

$$\frac{\chi''(\mathbf{q} + \mathbf{Q}, E)}{\omega} = \frac{\chi_0 \gamma}{(a^2 q^2)^2 + \gamma^2 E^2} \quad (8)$$

For these reasons, the measured linewidth does not become zero at the magnetic transition, but instead becomes a constant  $\delta_{\text{res}}$ . To capture this effect in a simple way, we considered a uniform shift of the linewidth,  $W = \xi^{-1} + \delta_{\text{res}}$ , with  $\delta_{\text{res}} = 0.11$  in both cases.

---

\* Electronic address: mcqueeneyrj@ornl.gov

- [1] S. O. Diallo, D. K. Pratt, R. M. Fernandes, W. Tian, J. L. Zarestky, M. Lumsden, T. G. Perring, C. L. Broholm, N. Ni, S. L. Bud'ko, P. C. Canfield, H.-F. Li, D. Vaknin, A. Kreyssig, A. I. Goldman, and R. J. McQueeney, Phys. Rev. B **81**, 214407 (2010).
- [2] H.-F. Li, C. Broholm, D. Vaknin, R. M. Fernandes, D. L. Abernathy, M. B. Stone, D. K. Pratt, W. Tian, Y. Qiu, N. Ni, S. O. Diallo, J. L. Zarestky, S. L. Bud'ko, P. C. Canfield, and R. J. McQueeney, Phys. Rev. B **82**, 140503(R) (2010).
- [3] G. S. Tucker, R. M. Fernandes, H.-F. Li, V. Thampy, N. Ni, D. L. Abernathy, S. L. Bud'ko, P. C. Canfield, D. Vaknin, J. Schmalian, and R. J. McQueeney, Phys. Rev. B **86**, 024505 (2012).
- [4] G. S. Tucker, R. M. Fernandes, D. K. Pratt, A. Thaler, N. Ni, K. Marty, A. D. Christianson, M. D. Lumsden, B. C. Sales, A. S. Sefat, S. L. Bud'ko, P. C. Canfield, A. Kreyssig, A. I. Goldman, and R. J. McQueeney, Phys. Rev. B **89**, 180503(R) (2014).
- [5] A. Zheludev, [www.neutron.ethz.ch/research/resources/reslib](http://www.neutron.ethz.ch/research/resources/reslib).
- [6] M. Ramazanoglu, J. Lamsal, G. S. Tucker, J.-Q. Yan, S. Calder, T. Guidi, T. Perring, R. W. McCallum, T. A. Lograsso, A. Kreyssig, A. I. Goldman, and R. J. McQueeney, Phys. Rev. B **87**, 140509(R) (2013).
- [7] R. M. Fernandes, A. V. Chubukov, J. Knolle, I. Eremin, and J. Schmalian, Phys. Rev. B **85**, 024534 (2011).